

# Size Effect in Hardened Cement Paste and High Strength Concrete

B.L.Karihaloo & H.M.Abdalla

Civil Engineering Division, Cardiff University, Cardiff CF24 0YF, UK

**ABSTRACT:** This paper will report on an experimental investigation into the size effect in the strength of hardened cement paste (HCP, nominal compressive strength 40 MPa) and high strength concrete (HSC, nominal compressive strength 110 MPa) as measured in three point bending. The aim of the investigation is to judge the range of applicability of the various size effect formulae available in the literature. With this aim in mind, the failure loads have been analysed according to the size effect formulae of Bazant and of Karihaloo for the notched beams and according to those of Bazant and of Carpinteri for the unnotched beams. The results of this analysis will be presented. Improvements to Karihaloo's size effect formula will also be proposed.

## 1 INTRODUCTION

The fracture mechanics size effect, as opposed to the Weibull statistical size effect, is a controversial topic in the fracture of concrete. Yet, it is fracture mechanics which alone can illuminate the hitherto unexplained size effect observed in the strength of concrete structures. It would therefore seem appropriate to conduct dedicated experiments in order to establish the range of applicability of the several fracture mechanical size effect formulae available in the literature (Bazant, 1984, 1997; Carpinteri, 1994a; Karihaloo, 1999).

Bazant (1984), using the energy release rate concept, proposed the formula

$$(\sigma_N)_u = A_1 \left(1 + \frac{B_1}{W}\right)^{-1/2} \quad (1)$$

where  $(\sigma_N)_u$  is the nominal stress at failure of a structure of specified shape and loading condition,  $W$  is a characteristic size of the structure, and  $A_1$  and  $B_1$  are positive constants. Bazant's formula reduces to the linear elastic fracture mechanics (LEFM) limit as  $W \rightarrow \infty$ . In fact, formula (1) has been established by Taylor's expansion from this asymptotic limit (Karihaloo, 1995).

Karihaloo (1999), using the stress intensity factor and the fictitious crack concepts, proposed the formula

$$(\sigma_N)_u = A_2 \left(1 - \frac{B_2}{W}\right)^{1/2} \quad (2)$$

where  $A_2$  and  $B_2$  are constants. This formula also reduces to the LEFM limit as  $W \rightarrow \infty$ . It is, however, unlikely to be applicable when  $W$  is small, which is a consequence of several approximations and assumptions made in its derivation. These will be touched upon later.

Many quasi-brittle structures are known to fail at crack initiation, although the process zone is well developed. For such structures the nominal failure stress was found to approach the LEFM limit for  $W \rightarrow \infty$  from above

$$(\sigma_N)_u = \left(A_3 + \frac{B_3}{W}\right)^{1/2} \quad (3)$$

Here,  $A_3$  and  $B_3$  are positive constants. This formula was obtained by Carpinteri and his co-workers using multifractal scaling concepts (Carpinteri, 1994a, 1994b; Carpinteri and Ferro, 1994). Bazant (1997) also obtained a size effect formula for initially-unnotched structures using the same concepts as for the notched structures. That formula, however, differs from (3) in that the exponent is approximately equal to unity.

The aims of this paper are two-fold. First, it will compare the size effect formulae (1) and (2) for tests on hardened cement paste (HCP, nominal compressive strength 40 MPa) and high strength concrete (HSC, nominal compressive strength 110 MPa) with a view to identifying their ranges of applicability. Beams (span to depth ratio of 4) with depth varying between 50 mm and 400 mm with a central edge notch were tested in three point

bending. The notches ranged in depth from the very shallow (notch to depth ratio 0.05) to the deep (notch to depth ratio 0.5). Comparison will also be made of the size effect formulae for unnotched HSC beams ranging in depth between 50 mm and 400 mm.

The second aim of the paper is to eliminate most of the assumptions made in the derivation of formula (2) with a view to obtaining a better understanding of the stress redistribution in the fracture process zone and of its role in the size effect of concrete structures.

## 2 NOTCHED HCP AND HSC BEAMS

Tests were conducted on notched HCP beams of span to depth ratio 4 in three point bending. The notch to depth ratios were selected to be 0.05, 0.10, 0.30 and 0.50. Four beams were tested for each notch depth. All beams were 100 mm wide (B). The mechanical properties of HCP were measured on several specimens using standard procedures. The mean values (and coefficients of variation) of the mechanical properties are: compressive strength 42.3 MPa (12.8%), split cylinder strength 3.53 MPa (12.7%), modulus of elasticity 20.8 GPa (8.3%), and specific fracture energy 7.13 J/m<sup>2</sup> (15.6%).

The mean values of the nominal failure strength of the notched HCP beams ( $(\sigma_N)_u = P_u/(BW)$ ) are given in Table 1. It is worth reminding the reader that the actual failure strength in three point bending of a beam with span to depth ratio of 4 is  $\sigma_u = 6P/(BW)$ , so that  $(\sigma_N)_u = (\sigma_u)/6$ . They are compared in Figures 1-4 for the four notch to depth ratios ( $\alpha$ ) with the predictions of formulae (1) and (2). The constants in these formulae were determined in the usual manner.

Tests were also conducted on notched HSC beams (span to depth ratio 4, width B = 100 mm) in three point bending. The mean values (and coefficients of variation) of the measured mechanical properties are: compressive strength

108.8 MPa (3.2%), split cylinder strength 7.40 MPa (4.9%), modulus of elasticity 40.45 GPa (3.9%), and specific fracture energy 44.7 J/m<sup>2</sup> (8.7%).

Three beams were tested for each of the three notch to depth ratios ( $\alpha = 0.05, 0.10, 0.30$ ). For the smallest notch to depth ratio only two beam depths were tested. The mean values of the nominal failure strength are given in Table 2.

The nominal failure strengths are plotted in Figures 5-7 for the three notch depths and compared with formulae (1) and (2).

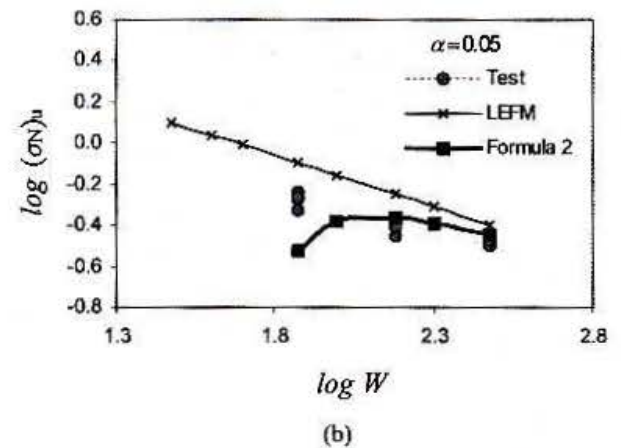
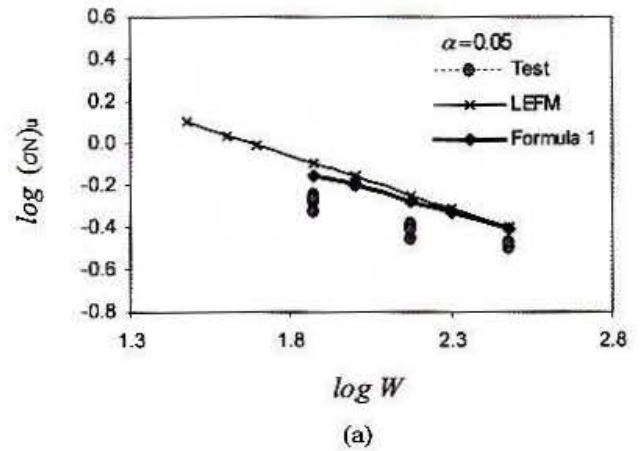


Figure 1. Size effect plot for HCP specimens with  $\alpha = 0.05$  according to formulae (1) and (2)

Table 1. Failure loads for HCP beams

W (mm)	$\alpha$	Mean $P_u$ (kN)	Mean $(\sigma_N)_u$ (MPa)
75	0.05	3.98	0.53
150		5.63	0.38
300		9.83	0.33
50	0.10	2.22	0.44
100		3.49	0.35
200		6.06	0.30
50	0.30	1.62	0.32
100		2.85	0.29
200		4.09	0.20
50	0.50	0.80	0.16
100		1.32	0.13
200		2.14	0.11

Table 2. Failure loads for HSC beams

W (mm)	$\alpha$	Mean $P_u$ (kN)	Mean $(\sigma_N)_u$ (MPa)
200	0.05	22.79	1.14
400		36.06	0.90
100	0.10	10.88	1.09
200		17.67	0.88
400		27.70	0.69
75	0.30	4.75	0.63
150		8.17	0.54
300		12.66	0.42

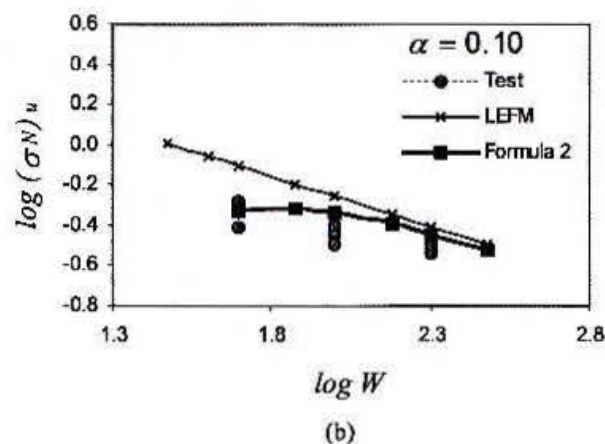
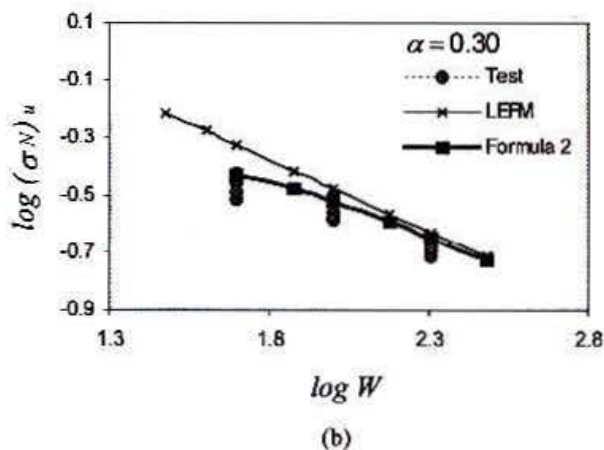
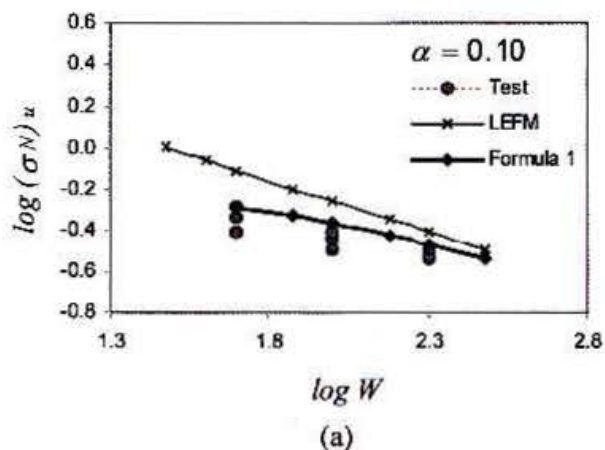


Figure 3. Size effect plot for HCP specimens with  $\alpha = 0.30$  according to formulae (1) and (2)

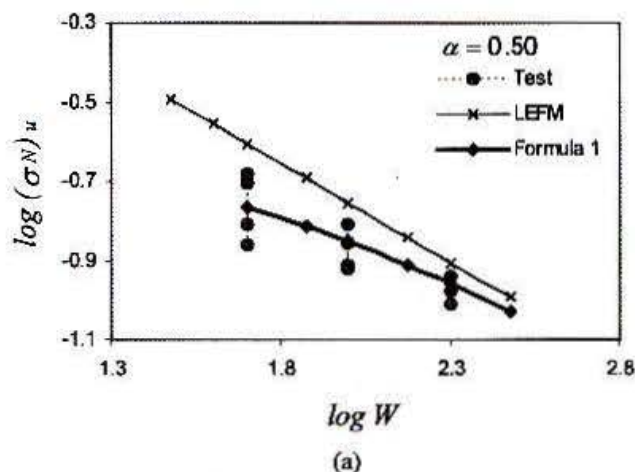


Figure 2. Size effect plot for HCP specimens with  $\alpha = 0.10$  according to formulae (1) and (2)

From the analysis presented in Figures 1-7, the following conclusions can be drawn.

- For notched HCP and HSC beams with notch to depth ratios of 0.05 and 0.10, the predictions of both formulae (1) and (2) deviate somewhat from the measured nominal strengths. The deviation of formula (2) for small sizes is particularly evident. The possible reasons for this will be discussed below.

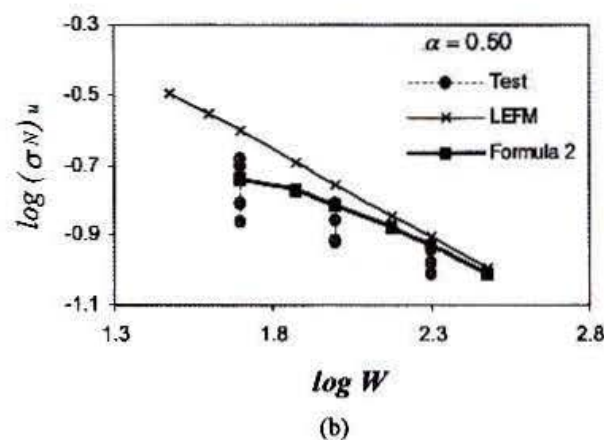
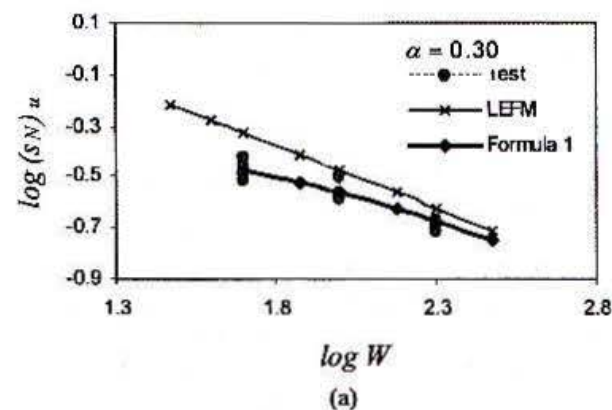


Figure 4. Size effect plot for HCP specimens with  $\alpha = 0.50$  according to formulae (1) and (2)



- For notched HCP beams with notch to depth ratio of 0.3 or more, both formulae (1) and (2) predict failure loads in good agreement with measured values for all sizes.
- For notched HSC beams with notch to depth ratio of 0.3 or more, the predictions of both formulae are again in good agreement with

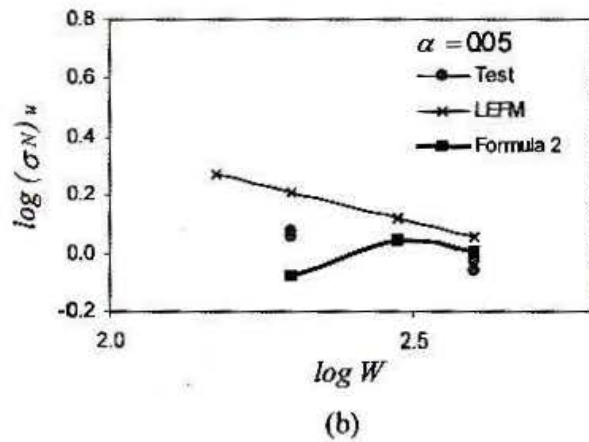
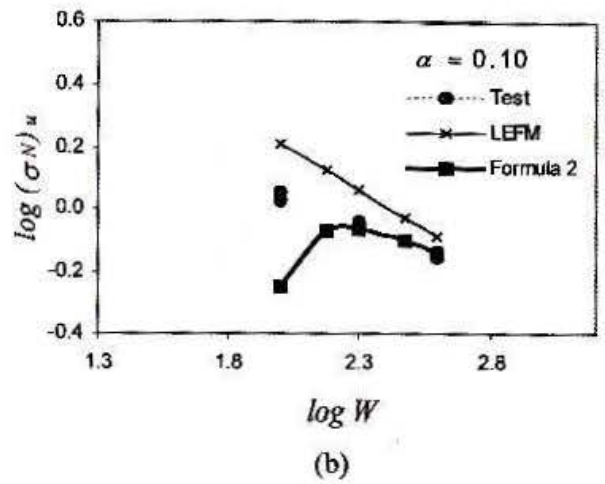
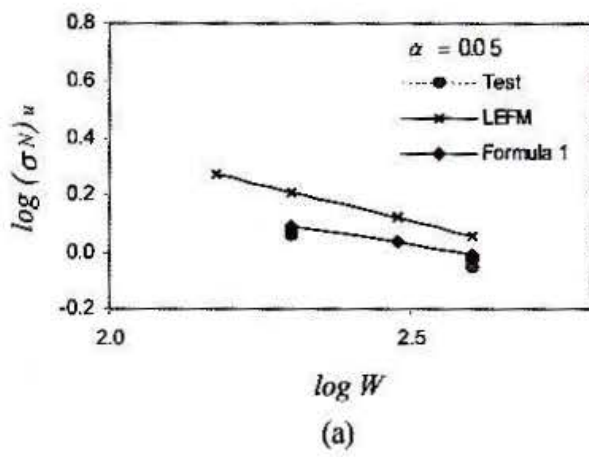


Figure 6. Size effect plot for HSC specimens with  $\alpha = 0.10$  according to formulae (1) and (2)

Figure 5. Size effect plot for HSC specimens with  $\alpha = 0.0$  according to formulae (1) and (2)

measured values for large sizes. However, somewhat surprisingly, formula (2) alone would appear to predict the correct trend for small sizes.

### 3 IMPROVEMENT OF FORMULA (2)

In the derivation of formula (2) (Karihaloo, 1999) it was recognised that quasi-brittle materials develop a diffuse fracture process zone (FPZ) before the

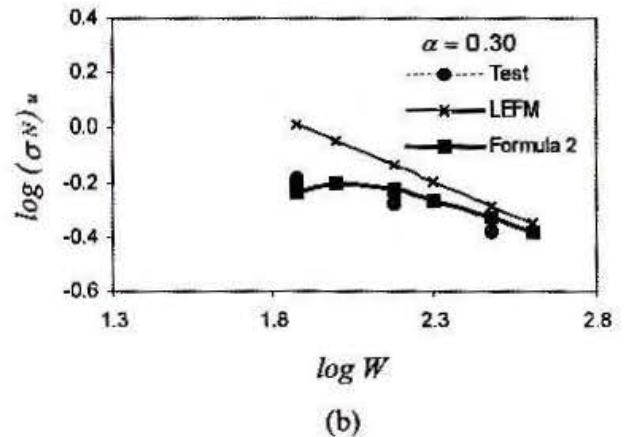
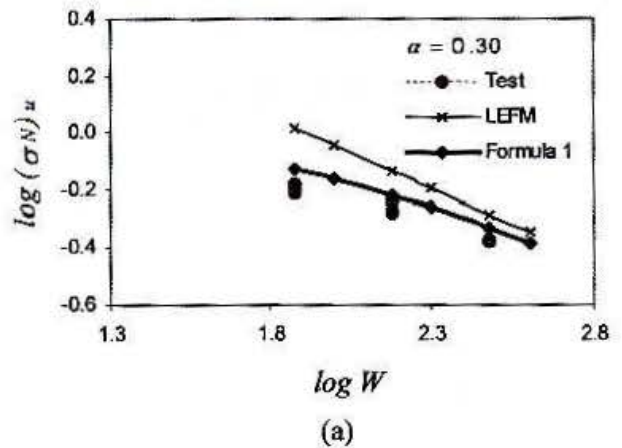
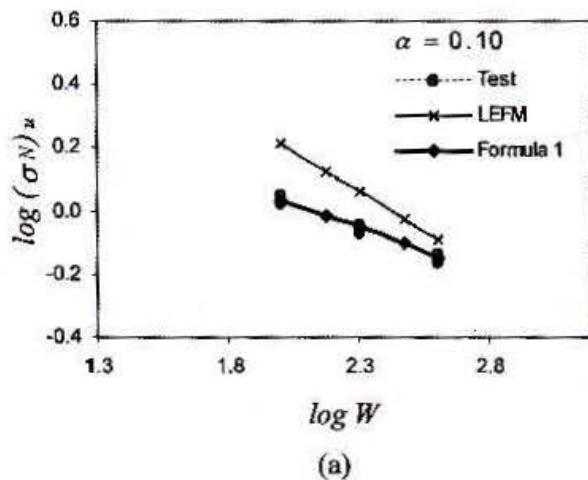


Figure 7. Size effect plot for HSC specimens with  $\alpha = 0.30$  according to formulae (1) and (2)



formation of a traction-free crack whose size can be commensurate with that of a small test specimen. Within this zone the stresses are redistributed so that it is necessary to consider not only the singular term in the asymptotic crack tip field but also higher order, nonsingular terms. In the derivation proper, Karihaloo (1999) used approximations for the higher order terms, as well as the weight (Green's)

functions for a semi-infinite crack in an infinite plane instead of a finite size crack in a finite three point bend (TPB) specimen. These approximations have been recently eliminated by taking into account accurate higher order terms of the crack tip asymptotic field, as well as by using the weight functions for a finite crack.

In common with the earlier derivation (Karihaloo, 1999), the traction-free crack with a FPZ of length  $\ell_p$  at its tip is decomposed into a traction-free crack (Figure 8) with the following stress field at its tip

$$\sigma_r(r) \equiv \sigma_0(r) = \frac{a_1}{\sqrt{r}} + 3a_3\sqrt{r} + 5a_5r^{3/2} \quad (4)$$

and the FPZ with the stress  $[\sigma(s) - \sigma_0(\ell_p - s)]$  and the displacement  $w(s)$  across its faces. In (4),  $a$  is related to the mode I stress intensity factor (SIF)  $K_I$  via  $a_1 = K_I / \sqrt{2\pi}$ . The coefficients  $a_1$ ,  $a_3$  and  $a_5$  depend on the crack length, applied load  $\sigma_r$  and size and geometry of the body. Solutions for TPB and a typical wedge-splitting geometry have been recently obtained by Karihaloo and Xiao (2001a,b).

For a TPB with a span to depth ratio of 4, the coefficients  $a_1$ ,  $a_3$ ,  $a_5$  are

$$a_1 = \sigma_r \sqrt{W} k_4(\alpha)$$

$$a_3 = \frac{\sigma_r}{\sqrt{W}} g_4^3(\alpha)$$

$$a_5 = \frac{\sigma_r}{W^{3/2}} g_4^5(\alpha)$$

where

$$k_4(\alpha) = \frac{\sqrt{\alpha} p_4(\alpha)}{\sqrt{2\pi} (1-\alpha)^{3/2} (1+3\alpha)}$$

$$p_4(\alpha) = 1.9 + 0.41\alpha + 0.51\alpha^2 - 0.17\alpha^3$$

$$g_4^1(\alpha) = 0.6534 - 9.2406\alpha + 49.515\alpha^2 - 153.97\alpha^3 + 233.48\alpha^4 - 148.73\alpha^5$$

$$g_4^2(\alpha) = 2.1491 - 52.998\alpha + 468.48\alpha^2 - 2084.4\alpha^3 + 4919.3\alpha^4 - 5869.4\alpha^5 + 2765.2\alpha^6$$

The displacement of the cohesive crack faces  $w(s)$  (representing the FPZ) can be expressed as the following singular equation

$$\int_0^{\ell_p} g(s,t) [\sigma(s) - \sigma_0(\ell_p - s)] ds = -w(t) \quad (5)$$

The finite tensile strength of concrete requires that SIF vanish at the FPZ tip. This in turn requires that the faces of FPZ close smoothly, i.e.

$$\int_0^{\ell_p} k(s) [\sigma(s) - \sigma_0(\ell_p - s)] ds = 0 \quad (6)$$

The weight functions  $g(s,t)$  and  $k(s)$  are the respective crack face opening displacement at the location  $t$  and the SIF at the crack tip of a single edge cracked specimen of finite size due to a pair of unit normal forces  $s$  on the crack faces (Figure 8). These have been derived by Xiao and Karihaloo (2001)

$$g(s,t) = -\frac{4}{\pi E'} \ln \left| \frac{\sqrt{s} - \sqrt{t}}{\sqrt{s} + \sqrt{t}} \right| + \frac{8}{E'} \left( A_1 \sqrt{t} - A_3 t^{3/2} + A_5 t^{5/2} \right) \quad (7)$$

$$k(s) = \sqrt{\frac{2}{\pi s}} + A_1 \sqrt{2\pi} \quad (8)$$

where  $E' = E$  for plane stress and  $E' = E / (1 - \nu^2)$  for plane strain. Accurate interpolation formulae for  $A_1$ ,  $A_3$  and  $A_5$  have been given by Xiao and Karihaloo (2001) which depend on the size and geometry of the body

$$\frac{A_i(\alpha, \gamma)}{W^{(i/2)+1}} = \sum_{j=0}^4 f_{ij}(\alpha) \gamma^j, \quad i=1,3,5 \quad (9)$$

where  $\alpha = a/W$ ,  $\gamma = s/a$  and  $a$  is the crack length.

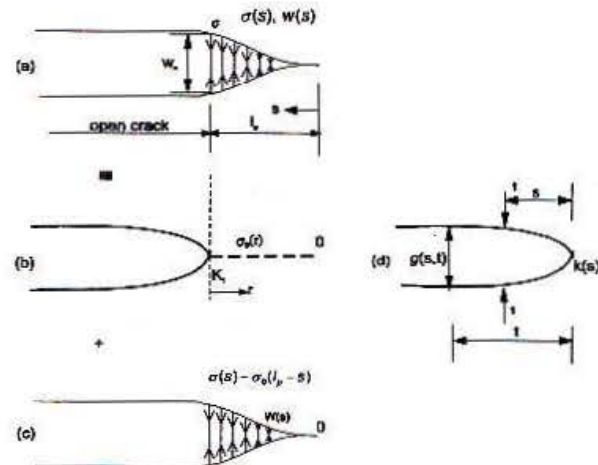


Figure 8. Decomposition of a traction free crack with a fracture process zone of length  $\ell_p$  (a) into the traction free crack with stress  $\sigma_0(r)$  ahead of crack tip (b) and the FPZ with stress  $[\sigma(s) - \sigma_0(\ell_p - s)]$  and displacement  $w(s)$ (c). As the faces close smoothly the stress intensity factor at 0 will vanish.  $k(s)$  is the stress intensity factor due to unit concentrated loads at  $s$ ,  $g(s, t)$  is the corresponding displacement at location  $t$  (d) (From Karihaloo, 1995)

The functions  $f_{ij}(\alpha)$  are

$$f_{14}(\alpha) = \left\{ \begin{array}{l} \frac{34.606\alpha^3 - 41.019\alpha^2 + 20.223\alpha - 3.7408}{(1-2\alpha)^2} \\ 0, \end{array} \right.$$

$$f_{13}(\alpha) = \begin{cases} \frac{-13.817\alpha^3 + 27.952\alpha^2 - 21.109\alpha - 4.8557}{(1-2\alpha)^3} \\ 0, \end{cases}$$

$$f_{52}(\alpha) = \begin{cases} \frac{19.996\alpha^3 - 17.901\alpha^2 + 5.595\alpha - 0.6524}{(1-2\alpha)^3 \alpha^2} \\ 129.03\alpha^3 - 204.66\alpha^2 + 108.13\alpha - 17.662, \end{cases}$$

$$f_{12}(\alpha) = \begin{cases} \frac{20.791\alpha^3 - 13.601\alpha^2 + 11.745\alpha - 3.9004}{(1-2\alpha)^2} \\ -3.2167\alpha^3 + 3.22\alpha^2 - 0.7748\alpha - 1.2004, \end{cases}$$

$$f_{51}(\alpha) = \begin{cases} \frac{-143.59\alpha^3 + 142.36\alpha^2 - 47.318\alpha + 5.3329}{(1-2\alpha)^3 \alpha^2} \\ \frac{-187.17\alpha^3 + 264.43\alpha^2 - 130.17\alpha + 21.167}{1-\alpha}, \end{cases}$$

$$f_{11}(\alpha) = \begin{cases} \frac{16.38\alpha^3 - 14.453\alpha^2 + 0.0025\alpha + 1.378}{(1-2\alpha)^2} \\ 127.17\alpha^3 - 157.39\alpha^2 + 73.588\alpha - 9.5209, \end{cases}$$

$$f_{50}(\alpha) = \begin{cases} 1.1667\alpha^3 + 4.045\alpha^2 - 3.0112\alpha + 0.3928, \\ -1.0667\alpha^3 - 5.335\alpha^2 + 4.4722\alpha - 0.9568, \end{cases}$$

$$f_{10}(\alpha) = \begin{cases} \frac{11.067\alpha^3 - 5.29\alpha^2 + 0.9753\alpha + 0.0354}{\alpha^2} \\ -6.3283\alpha^3 + 11.659\alpha^2 - 6.1031\alpha + 1.0268, \end{cases}$$

$$f_{14}(\alpha) = \begin{cases} \frac{2.4861\alpha^3 - 1.6212\alpha^2 - 0.0339\alpha + 0.1139}{(1-2.45\alpha)^3 \alpha^{3/2}} \\ 0, \end{cases}$$

$$f_{13}(\alpha) = \begin{cases} \frac{1.9089\alpha^3 - 3.0813\alpha^2 + 1.8375\alpha - 0.3641}{(1-2.45\alpha)^3 \alpha^{3/2}} \\ 0, \end{cases}$$

$$f_{52}(\alpha) = \begin{cases} \frac{-13.866\alpha^3 + 10.633\alpha^2 - 3.0231\alpha + 0.3968}{(1-2\alpha)\beta\alpha^{3/2}} \\ 7.2667\alpha^3 - 10.215\alpha^2 + 6.8468\alpha - 0.8862, \end{cases}$$

$$f_{51}(\alpha) = \begin{cases} \frac{251.04\alpha^3 - 234.57\alpha^2 + 75.35\alpha - 8.7819}{(1-2\alpha)^2} \\ -607.25\alpha^3 + 811.68\alpha^2 - 376.24\alpha + 56.809, \end{cases}$$

$$f_{50}(\alpha) = \begin{cases} \frac{3.2033\alpha^3 - 4.212\alpha^2 + 1.6762\alpha - 0.25}{1-2\alpha} \\ \frac{14.152\alpha^3 - 26.064\alpha^2 + 13.866\alpha - 2.3786}{\alpha}, \end{cases}$$

$$f_{54}(\alpha) = \begin{cases} \frac{0.0213\alpha^3 - 0.119\alpha^2 + 0.0904\alpha - 0.0185}{(1-2.45\alpha)^4 \alpha^3} \\ 0, \end{cases}$$

$$f_{53}(\alpha) = \begin{cases} \frac{-0.3963\alpha^3 + 0.5465\alpha^2 - 0.2519\alpha + 0.0388}{(1-2.01\alpha)^6 \alpha^3} \\ 0, \end{cases}$$

This work is still under progress, but the results are expected to be available at the time of the oral presentation of this paper.

In each of the above expressions except  $f_{53}(\alpha)$ , the first entry is for  $\alpha \leq 0.4$  and the second for  $\alpha > 0.4$ . In the expression of  $f_{53}(\alpha)$  the first entry is for  $\alpha \leq 0.5$  and the second for  $\alpha > 0.5$ .

#### 4 UNNOTCHED HSC BEAMS

A limited number of unnotched HSC beams were also tested in three point bending. The depth of these beams covered a wide range from 50 mm to 400 mm. All beams were 100 mm wide. The mean failure loads and nominal strength values are given in Table 3.

The mean nominal strength is plotted against the beam depth in Figure 9, together with the line of best fit. The odd values for depths 75 and 300 mm are presumably due to just one specimen being available for testing. The trend is, however, very clear - the strength reaches the asymptotic value for large sizes from above.

The measured values are compared in Figure 10 with the predictions of the multifractal scaling (MFSL) formula (3) due to Carpinteri. The constants  $A_3$  and  $B_3$  in this formula are calculated by a standard regression approach. Formula (3) but with the exponent  $\frac{1}{2}$  replaced by 1 also gives the nominal strength at crack initiation as obtained by Bazant (1997). The constants  $A_3$  and  $B_3$  are also determined by linear regression. The constant  $A_3$  represents the nominal strength for an infinitely large beam, whereas the constant  $B_3$  is related to the thickness of the so-called "boundary layer" of cracking. The Bazant modification of formula (3), denoted SEL, is also shown on Figure 10.

Table 3. Failure loads for unnotched HSC beams

W (mm)	Mean $P_u$ (kN)	Mean $(\sigma_N)_u$ (MPa)
50	9.40	1.88
75	11.90	1.59
100	16.40	1.64
150	24.45	1.63
200	30.40	1.52
300	41.53	1.38
400	56.50	1.41

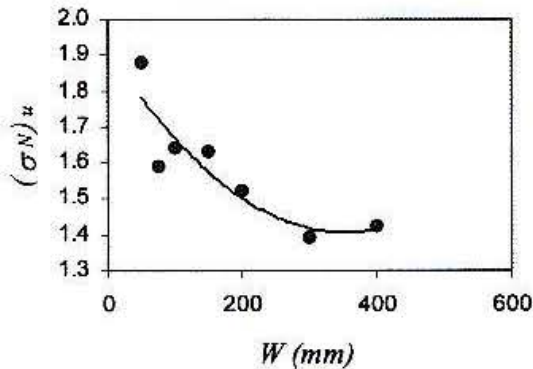


Figure 9. Variation in nominal failure strength with beam depth for unnotched HSC beams

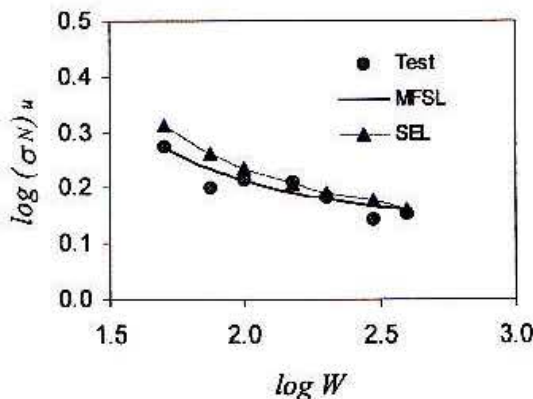


Figure 10. Size effect plots for unnotched TPB beams

For unnotched HSC beams, Carpinteri's formula (3) consistently gives better predictions than does Bazant's formula, although the difference in the predictions of the two is rather small.

## 5 CONCLUDING REMARKS

In conclusion, it must be pointed out that the above work did not contribute to a resolution of the controversy raging in the literature. In particular, it did not shed any light on why the strength of notched beams approaches the asymptotic limit for large sizes from below, whereas that of unnotched beams approaches it from above. However, preliminary results from the new theoretical work briefly described in Section 3 above show that there is a change in the curvature of the size effect plot

(i.e.  $\log (\sigma_N)_u$  vs  $\log W$ ) as the notch to depth ratio reduces towards zero. These results are most encouraging and, if confirmed by a detailed analysis, will be reported during the presentation.

## 6 ACKNOWLEDGEMENT

Financial support from the EPSRC under grant number GR/M78106 is gratefully acknowledged.

## 7 REFERENCES

- Bazant Z.P. 1984. Size effect in blunt fracture: concrete, rock, metal. *ASCE Journal of Engineering Mechanics*, 100:518-535.
- Bazant, Z.P. 1997. Scaling of quasi-brittle fracture: asymptotic analysis. *International Journal of Fracture*, 83: 19-40.
- Carpinteri, A. 1994a. Fractal nature of material microstructure and size effects on apparent mechanical properties. *Mechanics of Materials*, 18: 89-101.
- Carpinteri, A. 1994b. Scaling laws and renormalization groups for strength and toughness of disordered materials. *International Journal of Solids and Structures*, 31: 291-302.
- Carpinteri, A. & Ferro, G. 1994. Size effect on tensile properties: a unified explanation based on disorder and fractality of concrete microstructure. *Materials and Structures*, 27: 513-571.
- Karihaloo, B.L. 1995. *Fracture Mechanics and Structural Concrete*, Addison Wesley Longman, UK: 151-165.
- Karihaloo, B.L. 1999. Size effect in shallow and deep notched quasi-brittle structures. *International Journal of Fracture*, 95: 379-390.
- Karihaloo, B.L. & Xiao, Q.Z. 2001a. Higher order terms of the crack tip asymptotic field for a notched three-point bend beam, *International Journal of Fracture*, (submitted).
- Karihaloo, B.L. & Xiao, Q.Z. 2001b. Higher order terms of the crack tip asymptotic field for a wedge-splitting specimen, *International Journal of Fracture*, (submitted).
- Xiao, Q.Z. & Karihaloo, B.L. 2001. Approximate weight functions for singular and higher order terms of an edge crack in a finite plate, *Engineering Fracture Mechanics*, (submitted).